



HHS Public Access

Author manuscript

Cell Rep. Author manuscript; available in PMC 2022 August 20.

Published in final edited form as:

Cell Rep. 2022 August 09; 40(6): 111172. doi:10.1016/j.celrep.2022.111172.

Nano-organization of spontaneous GABAergic transmission directs its autonomous function in neuronal signaling

Natalie J. Guzikowski^{1,2}, Ege T. Kavalali^{1,2,3,*}

¹Department of Pharmacology, Vanderbilt University, Nashville, TN 37240-7933, USA

²Vanderbilt Brain Institute, Vanderbilt University, Nashville, TN 37240-7933, USA

³Lead contact

SUMMARY

Earlier studies delineated the precise arrangement of proteins that drive neurotransmitter release and post-synaptic signaling at excitatory synapses. However, spatial organization of neurotransmission at inhibitory synapses remains unclear. Here, we took advantage of the molecularly specific interaction of antimalarial artemisinins and the inhibitory synapse scaffold protein, gephyrin, to probe the functional organization of gamma-aminobutyric acid A receptor (GABA_AR)-mediated neurotransmission in central synapses. Short-term application of artemisinins severely contracts the size and density of gephyrin and GABA_AR γ 2 subunit clusters. This size contraction elicits a neuronal activity-independent increase in *Bdnf* expression due to a specific reduction in GABAergic spontaneous, but not evoked, neurotransmission. The same functional effect could be mimicked by disruption of microtubules that link gephyrin to the neuronal cytoskeleton. These results suggest that the GABAergic postsynaptic apparatus possesses a concentric center-surround organization, where the periphery of gephyrin clusters selectively maintains spontaneous GABAergic neurotransmission facilitating its autonomous function regulating *Bdnf* expression.

Graphical Abstract

This is an open access article under the CC BY-NC-ND license (<http://creativecommons.org/licenses/by-nc-nd/4.0/>).

*Correspondence: ege.kavalali@vanderbilt.edu.

AUTHOR CONTRIBUTIONS

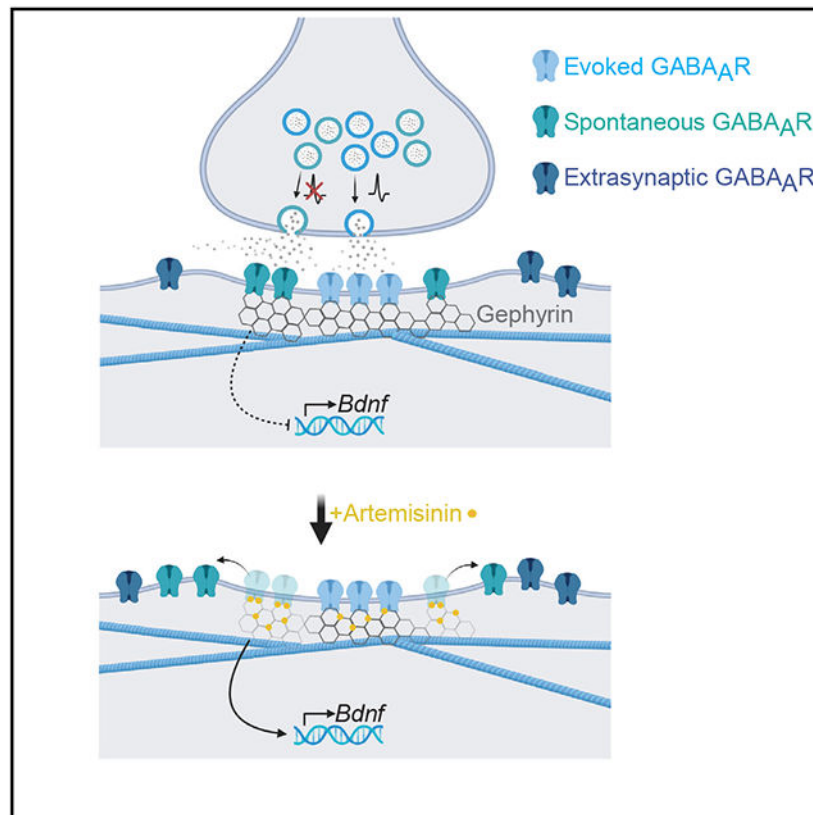
Conceptualization, N.J.G. and E.T.K.; methodology, investigation, and formal analysis, N.J.G.; interpretation, discussion, writing, and editing, N.J.G. and E.T.K.

SUPPLEMENTAL INFORMATION

Supplemental information can be found online at <https://doi.org/10.1016/j.celrep.2022.111172>.

DECLARATION OF INTERESTS

The authors declare no competing interests.



In brief

Guzikowski and Kavalali took advantage of the molecularly specific interaction of antimalarial artemisinins and an inhibitory synapse scaffold protein, gephyrin, to probe the functional organization of GABA_AR-mediated neurotransmission. Their study explores the nano-organization of the GABAergic synapse and the segregation of evoked and spontaneous neurotransmission.

INTRODUCTION

Over the past seven decades, our picture of synaptic neurotransmission has expanded to include both action potential-dependent release and spontaneous release, both of which have distinct physiological roles (Andreae and Burrone, 2018; Gonzalez-Islas et al., 2018; Kavalali, 2018). Extensive work has been conducted at the excitatory synaptic terminal delineating a precise transsynaptic alignment of molecular nanocolumns that drives the segregation of evoked and spontaneous release (Biederer et al., 2017; Guzikowski and Kavalali, 2021; Maschi and Klyachko, 2017; Ramsey et al., 2021; Tang et al., 2016). However, it remains unclear whether a similar nanostructure applies to inhibitory synapses as well. To date, a partial segregation of evoked and spontaneous release at the inhibitory synapse has been demonstrated, but how this segregation is achieved is unknown (Horvath et al., 2020). To address this question, we took advantage of a family of antimalarial small

molecule compounds, artemisinins, to probe the relationship of gamma-aminobutyric acid A receptor (GABA_AR) clustering and gephyrin.

Artemisinins are commonly used antimalarials, with gephyrin recently identified as a primary mammalian target, stimulating work delineating its effect on inhibitory neurotransmission (Li et al., 2017; Tu, 2016). Artemether and artesunate are semi-synthetic derivatives developed from the parent compound artemisinin, collectively referred to as artemisinins. Gephyrin is a scaffolding protein thought to mediate the mesophasic assembly of GABA_ARs at the synapse by forming a flexible hexagonal lattice at the inhibitory postsynaptic domain, analogous to the role of PSD95 at excitatory synapses (Choi and Ko, 2015; Liu et al., 2020). The explicit role of gephyrin in inhibitory receptor localization, stabilization, mobility, and retention is unclear, in part due to the extensive diversity in GABA_AR subunit composition (Farrant and Nusser, 2005; Jacob et al., 2005; Meier et al., 2001). While glycine receptors require gephyrin to localize at the synapse, only a subset of GABA_AR subunits demonstrate gephyrin colocalization and only a further subset, GABA_AR α 1, 2, 3, and 5, exclusively demonstrate direct gephyrin binding (Brady and Jacob, 2015; Essrich et al., 1998; Kasaragod et al., 2019; Kneussel et al., 2001; Lévi et al., 2004; Maric et al., 2011). Crystal structures of the gephyrin E (GephE) domain revealed the universal binding pocket for GABA_ARs was shared by artemisinins, fostering a competitive interaction where artemisinins prevent GABA_ARs from binding to gephyrin (Kasaragod et al., 2019). Therefore, we used artemisinins as tool to disrupt GABA_AR-gephyrin interactions to delineate the role of gephyrin in distinct modes of neurotransmission.

In this study, we first demonstrate that parental artemisinin and artemether treatment cause a reduction in gephyrin cluster volume and density, primarily by shedding gephyrin monomers from the cluster periphery, while the number of inhibitory synaptic puncta is unchanged. Furthermore, this loss of gephyrin is paralleled by loss of GABA_AR γ 2 subunit expression. Surprisingly, artemisinin treatment has a marginal effect on action potential frequency but significantly increases *Bdnf* mRNA expression. Therefore, we investigated the different modes of GABAergic neurotransmission to uncover how *Bdnf* is regulated. We show that parental artemisinin and artemether cause a specific disruption to spontaneous GABAergic transmission, while all artemisinins show no effect on evoked activity. The disruption of GABA_AR-gephyrin binding with artemisinins leads to the suppression of spontaneous GABAergic transmission and reciprocal augmentation of tonic GABAergic inhibition, indicating a parallel increase in the population of extrasynaptic GABA_ARs. We then use nocodazole, a tubulin polymerization inhibitor, to investigate the role of downstream gephyrin-microtubule interactions. Collectively, our results suggest a center-surround organization of evoked and spontaneous release at the GABAergic post-synapse where gephyrin is dynamically required to anchor spontaneous-release specific GABA_ARs, maintaining their autonomous function regulating *Bdnf* expression.

RESULTS

Artemisinins decrease gephyrin cluster volume

We utilized primary hippocampal cultures to investigate the action of artemisinins at inhibitory synapses using immunocytochemistry and whole-cell voltage-clamp

electrophysiology (Figures 1A and 1B). Following 1-h treatment of neurons with artemisinins, coverslips were co-immunostained for inhibitory synapse markers. Inhibitory synaptic puncta were identified by the colocalization of an inhibitory presynaptic marker, vesicular gamma-aminobutyric acid (GABA) transporter (vGAT), and an inhibitory postsynaptic marker, gephyrin. These colocalizations were then normalized to dendritic length (MAP2) to quantify inhibitory synapse density. Artemisinins did not alter inhibitory puncta density, demonstrating that short-term treatment with artemisinins does not have a gross effect on inhibitory synapse number (Figures 1C and 1D). To further investigate the downstream effects of artemisinins, we used 3D direct stochastic optical reconstruction microscopy (dSTORM) to probe presynaptic, vGAT, and postsynaptic, gephyrin, clusters by analyzing single-molecule localizations. Protein clusters were defined as more than six gephyrin or vGAT molecules localized within 0.1 μm of each other (Figure 1E). Artemether and parental artemisinin treatment significantly reduced gephyrin cluster volume by approximately 40% with no effect on vGAT cluster volume, demonstrating a specific postsynaptic effect. Artesunate did not affect gephyrin cluster volume (Figures 1E-1G). To disentangle which region of a gephyrin cluster is lost following treatment, we measured the distance between the centers of the presynaptic vGAT and post-synaptic gephyrin juxtaposed clusters. This analysis reveals no change in the centroid distance (Figure 1H), consistent with gephyrin shedding from the periphery of the clusters (Figure 1I).

Artemisinins alter gephyrin cluster density

To further evaluate the effect of artemisinins, we quantified the density of gephyrin in concentric circles from cluster center. Previous reports have demonstrated that gephyrin displays occasional subsynaptic clustering; consistent with these reports, the majority of gephyrin clusters we visualize are organized as a single domain (Crosby et al., 2019; Liu et al., 2020; Pennacchiotti et al., 2017). In the control group, as distance increases from the center, gephyrin density decreases, with the densest region being at the center. Furthermore, artemether and parental artemisinin significantly reduce density consistently at multiple 5-nm annuli, with artesunate having a slight downward trend at select radii (Figure 2B; Table S1). Evaluating density at variable distances from cluster center not only provides insight into innate clustering characteristics of gephyrin but further demonstrates artemether and parental artemisinin's specific disruption of gephyrin clustering.

To further understand how the clustering of gephyrin changed independent of absolute density and cluster shape, we calculated the pair correlation function for individual gephyrin clusters normalized to the theoretical fit (Hartley et al., 2015; Sengupta et al., 2013). This analysis allows clustering changes to be compared between groups with $g(r) > 1$ representing a heterogeneous organization (i.e., clustering), $g(r) = 1$ a uniform random distribution, and $g(r) < 1$ a molecularly de-enriched area (Tang et al., 2016). In all groups, point pattern information over a 300-nm radius from cluster center has the same trend as absolute density, heightened clustering at the center and dispersion toward the periphery (Figure 2C). The radii at which $g(r)$ is no longer greater than 1 is the transition from substantial protein clustering to a more dispersed molecular arrangement at approximately 75 nm for DMSO, 60 nm for artemether, 50 nm for parental artemisinin, and 70 nm for artesunate (Figures 2D-2F). Thus, these results suggest that and parental artemisinin induce

a reduction in gephyrin cluster density causing a decrease in cluster volume due to the selective loss of the periphery.

Functional impact of artemisinin treatment

Based on the interdependent relationship between gephyrin and GABA_ARs, we next investigated the consequence of this reduction in peripheral gephyrin volume on GABA_AR subunit expression (Craig et al., 1996; Essrich et al., 1998; Kneussel et al., 2001; Lévi et al., 2004). The GABA_AR γ 2 subunit is crucial in mediating the clustering dynamics of GABA_ARs, with α 1, β 2, γ 2 the predominant subunits composing the pentameric GABA_ARs (Allred et al., 2005; Farrant and Nusser, 2005; Kneussel et al., 1999, 2001; Lévi et al., 2004; Sperk et al., 1997). In control and parental artemisinin treatment groups, the clustering dynamics of GABA_AR γ 2 subunit single-molecule localizations parallel that of gephyrin, whereby parental artemisinin caused a significant reduction in GABA_AR γ 2 subunit cluster surface area and increased sphericity (Figures 3A-3C).

Next, we aimed to test the functional impact of this structural manipulation. When we monitored action potential firing using whole-cell current clamp experiments, we detected only a marginal effect of the reduction in gephyrin and GABA_AR γ 2 clustering on intrinsic neuronal excitability with a slight decrease in firing rate, without a significant effect on resting membrane potential or the amplitudes of sub-threshold excitatory postsynaptic potentials (EPSPs) (Figures 3D-3G). In contrast, parental artemisinin treatment resulted in a significant increase in *Bdnf* mRNA expression, whereas an absolute suppression of activity for 1-h (tetrodotoxin [TTX] treatment) has no effect (Figures 3H and 3I). These results demonstrate an activity-independent increase in *Bdnf* expression following artemisinin treatment. To elucidate the mechanism mediating this increase in *Bdnf*, in the subsequent sets of experiments, we further probed action potential-dependent and -independent modes of GABAergic neurotransmission.

Artemisinins suppress spontaneous GABAergic transmission

This reduction in gephyrin cluster volume and density led us to explore the functional consequences of artemisinins at the synapse. Previously, artemisinins' actions on glycinergic neurotransmission were investigated in human embryonic kidney (HEK) cells. HEK cells transfected with gephyrin and glycine receptors had reduced glycine-induced currents when treated with both parental artemisinin and its derivative artemether. In addition, parental artemisinin and artemether reduced glycine whole-cell currents in spinal cord neurons (Kasragod et al., 2019). However, the results of whole-cell agonist-induced currents cannot be fully extrapolated to central synapses as they do not recapitulate physiological neurotransmission. Therefore, we performed whole-cell voltage-clamp electrophysiology on hippocampal neurons to monitor GABAergic neurotransmission and examine how the shrinkage of gephyrin clusters affects neurotransmission.

One-hour treatment of hippocampal neurons with artemether and parental artemisinin significantly reduced miniature inhibitory postsynaptic current (mIPSC) frequency relative to vehicle, dimethyl sulfoxide (DMSO) incubation. Consistent with its lack of effect on gephyrin cluster size, artesunate had no effect on mIPSC frequency after 1-h treatment.

However, longer-term treatment (24 h) with artesunate also resulted in a substantial decrease in mIPSC frequency (Figures 4A and 4B). Interestingly, this robust decrease in mIPSC frequency was accompanied by only a slight decrease in mIPSC amplitudes, suggesting a potential loss of a specific subgroup of receptors rather than a global reduction in receptor density (Figures 4C-4F). To further disentangle the relationship of mIPSC frequency and amplitudes following artemisinin treatment, we employed time-domain denoising analysis, previously used to analyze fluorescence signals and electrophysiological single-channel recordings (Chanaday, 2018; Chanaday and Kavalali, 2018; Chung and Kennedy, 1991). This analysis assisted us in recovering smaller-amplitude mIPSC events lost in baseline noise and resulted in a positive correction in average frequency of mIPSCs seen after treatment. The inclusion of these events also decreased average amplitude following denoising, and it induced a consistent left-ward shift in mIPSC amplitude distribution (Figure S1).

When artemisinins are not included in the bath following pre-incubation, the decrease in mIPSC frequency is not as robust, implying a competitive relationship between GABA_ARs and artemisinins (Figures 4G-4I). These results are consistent with the action of engineered peptides that exhibit competitive attachment to the gephyrin receptor binding pocket, as at low concentrations they reduce glycine mIPSC frequency with no change in mIPSC amplitudes (Maric et al., 2017). The marginal effect of artesunate on gephyrin cluster volume and density in combination with unaltered mIPSC frequency corroborates the interplay of imaging results and the electrophysiology phenotype. Artesunate likely does not have an acute effect on gephyrin cluster volume or mIPSC frequency due to within-family differences in GephE domain binding (Kasaragod et al., 2019).

The decrease in mIPSC frequency could be attributed to a decrease in neurotransmitter release rather than dispersion of GABA_ARs. To investigate if there is a presynaptic effect of artemisinins, we treated cells with a sub-saturating dose of the low-affinity antagonist (1,2,5,6-tetrahydropyridine-4-yl) methylphosphinic acid (TPMPA). Due to the low affinity of TPMPA for GABA_ARs, TPMPA will reduce mIPSC amplitude based on a concentration-dependent competition with endogenous GABA, allowing us to estimate GABA release based on the degree to which TPMPA reduces mIPSC amplitude (Vaden et al., 2020). Cells were pre-treated with artemisinins and then TPMPA was perfused during mIPSC recordings (Figures 4J and 4K). TPMPA perfusion reduced mIPSC amplitude to the same degree in all treatment groups, ~30%, demonstrating that quantal GABA release is unaltered following treatment with artemisinins (Figure 4L). Importantly, the effect of artemisinins is inhibitory synapse specific as treatment had no effect on miniature excitatory postsynaptic current (mEPSC) frequency or amplitude (Figures 4M-4O), further supporting the specificity of the effect on gephyrin.

Artemisinins do not alter GABAergic evoked neurotransmission

Following our investigation into mIPSCs, we further probed inhibitory neurotransmission by investigating evoked release. Due to the robust decrease in mIPSC frequency following parental artemisinin and artemether treatment, we expected to see similar alterations in evoked release. Surprisingly, there was no difference in evoked inhibitory postsynaptic

current (eIPSC) amplitudes between groups (Figures 5A and 5B). Upon repetitive stimulation — 10 action potentials at 10 Hz (100 ms ISI) or 20 Hz (50 ms ISI) — synapses treated with artemisininins depressed to the same degree as controls, demonstrating that artemisininins did not affect release probability (Figures 5C-5E). Thus, treatment with artemisininins preferentially dysregulates spontaneous neurotransmission as opposed to evoked neurotransmission, suggesting acute disruption of gephyrin impairs spontaneous-release-specific GABA_ARs.

Artemisininins augment GABA_A currents mediating tonic inhibition

Following our investigation into spontaneous and evoked neurotransmission, we examined tonic inhibition, a mode of neural communication regulating cell excitability. Tonic inhibition is neurotransmission mediated by extrasynaptic GABA_ARs activated by the low concentration of GABA in the extracellular space. The stochastic opening of extrasynaptic GABA_ARs results in tonic current that is often described as “noise” during voltage-clamp recordings (Farrant and Nusser, 2005). We quantified this tonic inhibition by examining the distribution of current around the mean, whereby a Gaussian distribution with a lower standard deviation represents less noise and thus reduced tonic inhibition. At baseline, artemether and parental artemisinin, both of which reduced mIPSC frequency, generated significantly greater noise than DMSO (Figures 6B and 6C). After recording baseline tonic current for each treatment group, we perfused TPMPA, which remarkably reduced tonic current to comparable levels in all groups (Figures 6D-6H). Furthermore, we also see a positive shift in the holding current in the artemether and parental artemisinin groups, with more than a 20% decrease in holding current upon TPMPA perfusion, suggesting a greater amount of tonic current. To further confirm our measurement of GABA-mediated tonic current, opposed to another source of noise, we measured the effect of the common GABA_AR antagonist, bicuculline, on the control group (Figures 6D and 6E). Overall, this assessment suggests that there is an increase in the number of receptors that mediate tonic current.

Disruption of microtubule interaction mimics artemisininins' action

Our results indicate that the disruption of GABA_AR-gephyrin binding preferentially disrupts spontaneous GABAergic neurotransmission. Therefore, we further probed this apparent center-surround organization of evoked and spontaneous neurotransmission via the distribution of microtubules, downstream of the GABA_AR-gephyrin interaction. Gephyrin stabilizes the inhibitory postsynapse and decreases receptor mobility by anchoring to microtubules in the inhibitory postsynaptic cytoskeleton (Kirsch and Betz, 1995; Kirsch et al., 1991; Sassoè-Pognetto et al., 2011). The application of nocodazole, which disrupts microtubules by preventing the normal balance of microtubule assembly and disassembly, allowed us to investigate how inhibitory neurotransmission is regulated downstream of GABA_AR anchoring. The effect of nocodazole was tested in a dose-dependent manner whereby, at 1-h of 10 µg/mL (33 µM) treatment, microtubules were severely disrupted and gephyrin puncta size was reduced (Figures 7A-7D). This dose is consistent with earlier studies where 10 µg/mL led to a significant decrease in tubulin immunostaining after 30 min and microtubule destruction after 4 h (Ligon and Steward, 2000; Meyer et al., 2000). Following nocodazole treatment, mIPSC frequency was significantly reduced with

the selective loss of smaller-amplitude mIPSCs (Figures 7E-7H). To further elucidate the subgroup of GABA_ARs disrupted by artemisinins, neurons were treated with both parental artemisinin and nocodazole. Here, the combined treatment with parental artemisinin and nocodazole did not result in a further decrease in frequency (Figure 7I). These results indicate that disrupting microtubules affects the same population of GABA_ARs that are disrupted following artemisinin treatment, demonstrating gephyrin binding to microtubules as an essential mediator of GABA_AR synaptic localization. Similar to artemisinin treatment, eIPSC amplitudes were unaltered between control and nocodazole-treated groups (Figures 7J and 7K). In addition, repetitive stimulation—10 action potentials at 10 Hz and 20 Hz—caused the same degree of depression in all groups (Figures 7L-7N).

DISCUSSION

Synapses maintain action potential-dependent and spontaneous modes of neurotransmission through distinct pre- and postsynaptic mechanisms instilling distinct kinetics, pathways, and physiological roles to different modes of release. Extensive work at excitatory synapses via the application of use-dependent drugs and optical imaging have demonstrated the segregation of spontaneous and evoked neurotransmission (Atasoy et al., 2008; Melom et al., 2013; Peled et al., 2014; Reese and Kavalali, 2016; Sara et al., 2011). The distinct functional roles of evoked and spontaneous release at excitatory synapses provides a rationale for robust segregation maintained by prominent nano-organization within single active zones that link pre- and postsynaptic compartments (Biederer et al., 2017; Guzikowski and Kavalali, 2021; Maschi and Klyachko, 2017; Tang et al., 2016). However, due to the unique structure and function of inhibitory synapses, the same properties cannot be assumed for inhibitory neurotransmission but should be thoroughly investigated. Studies at excitatory synapses have created a picture of a molecularly heterogeneous synapse, where active-zone nanostructure aligns with postsynaptic receptor organization creating a precise transsynaptic alignment of release sites and receptors shaping synaptic efficacy, determining neurotransmission reliability, and tuning plasticity (Kusick et al., 2020; Li et al., 2021; Ramsey et al., 2021; Tang et al., 2016). However, only recently has a partial segregation of evoked and spontaneous release been shown at the inhibitory synapse. The use of picrotoxin, a use-dependent GABA_AR channel blocker, demonstrated that approximately 40% of GABA_ARs are exclusively activated by evoked release (Horvath et al., 2020). The intracellular postsynaptic binding site of artemisinins allowed us to disrupt intrinsic synaptic structural elements and directly probe the cytosolic mechanisms that might mediate this segregation. In our experiments following acute treatment with artemisinins, the shrinkage of gephyrin cluster volume in concert with a decrease in mIPSC frequency point to the specific loss of gephyrin-dependent spontaneous-release-specific GABA_ARs mediating *Bdnf* transcription (Figure 7O).

Gephyrin was proposed as the central organizer of the inhibitory synapse; however, the importance of gephyrin in synaptic receptor organization and inhibitory synaptic development is complex. Unlike glycine receptors that show an absolute dependence on gephyrin, the extensive subunit heterogeneity of GABA_ARs (19 subunits) makes it challenging to delineate receptor dependence on gephyrin and how this mediates synaptic and extrasynaptic receptor localization (Farrant and Nusser, 2005; Lévi et al., 2004; Sassoè-

Pognetto et al., 2000). Classically, receptors containing $\gamma 2$ and $\alpha 1, 2$, or 3 subunits are described as predominately synaptic, whereas $\alpha 4, 5$, and 6 are predominately extrasynaptic, with δ subunits purely extrasynaptic (Farrant and Nusser, 2005). In our experiments, the competitive interaction of GABA_ARs and artemisinins for the gephyrin universal binding pocket altered GABAergic neurotransmission and demonstrated the localization of GABA_ARs mediating spontaneous neurotransmission at the periphery of gephyrin clusters. In parallel with the loss of spontaneous GABAergic neurotransmission, treatment caused an increase in tonic inhibition consistent with the notion that GABA_ARs that mediate spontaneous transmission were shuttled toward extrasynaptic sites. Furthermore, we see that GABA_AR $\gamma 2$ subunit expression mimics that of gephyrin, whereby peripheral synaptic clustering of $\gamma 2$ is lost following treatment. Last, this physical disruption to the inhibitory synapse revealed a functional role of GABAergic spontaneous release in *Bdnf* regulation. These observations agree with the premise that gephyrin canonically regulates the dynamics of inhibitory receptors at the synapse as the absence of gephyrin increases receptor mobility and decreases receptor clustering without an absolute change in the number of receptors expressed on the membrane (Jacob et al., 2005; Meier et al., 2001). In addition, GABA_AR dynamics are regulated by the diffusion of receptors from extrasynaptic locations but not their insertion (Thomas et al., 2005). Moreover treatment with gephyrin super-binding peptides, engineered peptides that exhibit competitive binding to the gephyrin receptor binding pocket, reduces synaptic and increases extrasynaptic localizations of GABA_AR $\alpha 2$, demonstrating receptor dispersion as opposed to internationalization (Maric et al., 2017). These data suggest a model where, upon treatment with artemisinins, GABA_ARs move out of the synapse and into the extrasynaptic space due to decreased gephyrin binding. However, our findings do not fully exclude the possibility that GABA_ARs could be targeted for endocytosis and/or degradation following disruption of gephyrin binding.

The selective effect of artemisinin treatment on a subpopulation of GABA_ARs was bolstered by experiments with disrupted microtubule polymerization downstream of the GABA_AR-gephyrin interaction. Here, we used nocodazole as a tool to impair anchoring of gephyrin to the cytoskeleton, ultimately resulting in the same phenotype as artemisinins as indicated by mIPSC and eIPSC recordings. The surprising maintenance of evoked neurotransmission following artemisinins and nocodazole treatment suggests that these distinct forms of neurotransmission are spatially segregated.

The results of these studies have two possible explanations; either only the subpopulation of GABA_ARs that mediate spontaneous neurotransmission demonstrate gephyrin dependence, suggesting other clustering mechanisms, or density differences within gephyrin clusters cause the loss of the periphery first, allowing selective disruption of spontaneous neurotransmission. Experiments based on genetic knockout and viral-mediated knockdown of gephyrin suggest gephyrin is important for the confinement and clustering of only a subgroup of GABA_ARs subunits. In these studies, gephyrin loss of function specifically reduces $\alpha 2$, $\alpha 3$, $\beta 2/3$, and $\gamma 2$ clustering, suggesting alternative mechanisms of synaptic localization and clustering for the remaining subunits (Hausrat et al., 2015; Jacob et al., 2005; Kneussel et al., 2001; Lévi et al., 2004). Of note, the $\alpha 1$ subunit is unaffected following gephyrin knockout despite its ability to bind to the gephyrin universal binding site (Kneussel et al., 2001; Lévi et al., 2004; Maric et al., 2011). Overall, loss-of-function studies

to date have been unable to paint a clear picture of the relationship between gephyrin and neurotransmission (Kneussel et al., 1999; Lévi et al., 2004; Yu et al., 2007; van Zundert et al., 2005). Here, we disrupted gephyrin interactions acutely using artemisinin, which allowed us to rapidly probe the innate structure of the inhibitory postsynaptic apparatus. The reduced density of gephyrin molecules at the periphery of clusters made the edges of these clusters more vulnerable to artemisinin, causing the overall shrinkage of gephyrin clusters upon treatment. This allowed us to use artemisinin as a tool to specifically disrupt peripheral gephyrin GABA_AR binding and probe the spatial organization within the inhibitory synapse. In this setting, gephyrin cluster centers were maintained despite disruption of the cluster periphery, presumably due to elevated gephyrin density within the centroid region. We posit that this apparent differential effect of artemisinin treatment allowed for the preservation of evoked neurotransmission and the selective disruption to spontaneous neurotransmission likely irrespective of potential subunit differences in the center versus the periphery. We do not rule out the notion that specific GABA_AR subunits could display a heterogeneous organization within the synapse; however, our experiments focus on the relationship between structural elements and neurotransmission. Ultimately, our results reveal a center-surround organization of evoked and spontaneous neurotransmission (Figure 7O).

Historically the main role of inhibitory signaling has been cast as modulating excitatory neurotransmission and regulating a neuron's propensity to fire action potentials. Only recently has the biochemical signaling of inhibitory neurotransmission been addressed due to the few known targets of chloride. The discovery that with-no-lysine kinases (WNKs) function as chloride sensors mediating second-messenger cascades downstream of GABAergic chloride current provides insight into the dynamic nature of the inhibitory synapse (Chen et al., 2019; Heubl et al., 2017; Piala et al., 2014). A recent study demonstrated that the blockade of spontaneous GABAergic release alters calcium signaling and leads to multiplicative downscaling at excitatory synapses via *Bdnf* transcription. However, whether this happens physiologically in the presence of activity was unknown (Horvath et al., 2021). Our findings suggest that gephyrin mediates the nano-segregation of spontaneous and evoked neurotransmission facilitating the autonomous role of GABAergic spontaneous neurotransmission in the regulation of *Bdnf* transcription. Our ability to selectively disrupt spontaneous neurotransmission and see a subsequent increase in *Bdnf* implies *Bdnf* is a regulated specific target of spontaneous GABAergic release. Our current findings demonstrate the inhibitory synapse is more dynamic than previously thought and structural mechanisms to facilitate the segregation of evoked and spontaneous release are in place. Different pathways that can drive, maintain, and regulate different modes of neurotransmission imply distinct functional roles with molecular segregation, providing a platform to mediate these biochemical pathways.

Limitations of the study

In this study, we probe the functional and structural nano-organization of inhibitory GABAergic synapses in primary hippocampal cultures. While this is a common model system to study synaptic nanostructure and physiology, further work in other model systems and *in vivo* is necessary to fully elucidate inhibition's role in neural circuits. The

demonstrated segregation of evoked and spontaneous GABA-mediated neurotransmission highlights the diverse functional roles for distinct modes of inhibitory neurotransmission. While the use of artemisinin allowed us to probe the downstream role of spontaneous GABAergic neurotransmission in regulating *Bdnf* gene transcription, further work is necessary to causally link GABA release and downstream signaling pathways. Furthermore, while pharmacological manipulation with artemisinin acted as a great tool to study GABAergic synapse nanostructure, the field would greatly benefit from high-quality optical tools that sense GABA and chloride to further untangle inhibitory synapse nanostructure.

STAR★METHODS

RESOURCE AVAILABILITY

Lead contact—Further information and requests for resources and reagents should be directed to and will be fulfilled by the lead contact, Ege T. Kavalali (ege.kavalali@vanderbilt.edu).

Materials availability—This study did not generate new reagents.

Data and code availability

- Microscopy data reported in this paper will be shared by the lead contact upon request.
- No original code has been generated in this study. Denoising code is available on github (Chanaday, 2018).
- Any additional information required to reanalyze the data reported in this paper is available from the lead contact upon request.

EXPERIMENTAL MODEL AND SUBJECT DETAILS

Animals—Sprague-Dawley rats of either sex (postnatal day 1–2) were used to generate primary hippocampal cultures, used in all experiments. All animal procedures were performed in accordance with the guide for the care and use of laboratory animals and were approved by the Institutional Animal Care and Use Committee at Vanderbilt University.

Cell culture—Dissociated hippocampal cultures were prepared as previously explained in (Kavalali et al., 1999). Briefly, hippocampi were dissected from P1-2 rats in 20% FBS containing Hank's balanced salt solution. Tissue was then washed and treated with 10 mg/mL of trypsin and 0.5 mg/mL DNase for 10 minutes at 37°C. Following trypsinization tissue was washed again and mechanically dissociated. Cells were then plated on 1:50 MEM:Matrigel coated glass coverslips. Neurons were incubated for the first 24hrs in media containing: MEM (no phenol red), 5 g/D-glucose, 0.2 g/L NaHCO₃, 0.1 g/L transferrin, 10% FBS, 2 mM L-glutamine and 20 mg/L insulin. On DIV 1 media was changed to growth media with 5% FBS, 0.5 mM L-glutamine, no insulin, and the addition of B27 supplement and 4 μM cytosine arabinoside. On DIV 4 growth media was changed to contain only 2 μM cytosine arabinoside. Cells were maintained at 37°C in a 5% CO₂ atmosphere until DIV 14–18 for experiments.

METHOD DETAILS

Drug treatment—Stock solutions of Artemether (50 mM), Artemisinin (175 mM), and Artesunate (65 mM) were created by dissolving the drugs in Dimethyl Sulfoxide (DMSO) and storing at room temperature. Working solutions of 10 mM were created the day of experiments. Primary hippocampal cultures were treated with 50 μ M of Artemether, Artemisinin, and Artesunate. Control samples were treated with the equivalent volume of DMSO. Coverslips were treated for 1 h with Artemisinins before electrophysiology, immunolabeling, and RNA extraction experiments and the respective drug was included in the bath solution, unless otherwise stated.

Stock solution of nocodazole (10 mg/mL) was prepared and stored at -20°C . Primary hippocampal cultures were treated with 10 μ g/mL (33 μ M), unless otherwise stated. Coverslips were treated for 1 hour with nocodazole before electrophysiology and immunolabeling experiments and nocodazole was included in the bath solution, unless otherwise stated.

Stock solution of (1,2,5,6-Tetrahydropyridine-4-yl) methylphosphinic acid (TPMPA) (50 mM) was prepared with milliQ water. Baseline mIPSCs were recorded for three minutes and then primary hippocampal cultures were perfused with tyrode's solution containing the respective Artemisinin and 200 μ M TPMPA. The bath was able to equilibrate for three minutes and then mIPSCs were recorded.

Electrophysiology—Whole cell patch clamp electrophysiology was performed on pyramidal cells at room temperature. For voltage clamp experiments cells were held at -70 mV. For current clamp experiments no current was injected. All recordings were performed following a two-minute equilibration period after breaking into the cell. Recordings were 3–5 minutes in length. eIPSCs were elicited via bipolar electrodes (FHC) immersed in the external bath solution with 35 mA stimulation as previously reported in published molecular neuroscience and electrophysiology experiments. Action potentials and eIPSCs were analyzed using Clampfit10 software (Molecular Devices). mIPSCs and mEPSCs were analyzed using MiniAnalysis software (Synaptosoft). Denoising analysis was conducted using a custom MATLAB script adapted from previous work in our lab (Figure S1) (Chanaday, 2018; Chanaday and Kavalali, 2018). Extracellular bath Tyrode's solution contained 150 mM of NaCl, 4 mM KCl, 10 mM of glucose, 10 mM of HEPES, 1.25 mM of MgCl₂, 2 mM of Ca²⁺ at pH 7.4 and 320 mOsm. For current clamp experiments no drugs were included in the bath solution. Intracellular pipette solution contained 110 mM K-Gluconate, 20 mM KCl, 10 mM NaCl, 10 mM HEPES, 4 mM Mg-ATP, 0.3 mM GTP, 0.6 mM EGTA at pH 7.3 and 284 mOsm. To isolate mEPSCs 1 mM TTX, 50 mM PTX, and 50 mM D-AP5 were included in the extracellular solution. To isolate mIPSCs 1 mM TTX, 10 mM CNQX, and 50 mM D-AP5 were included. To isolate eIPSCs 50 mM D-AP5 and 10 mM CNQX were added. Intracellular pipette solution contained 115mM Cs-methanesulphonate, 10mM CsCl, 5mM NaCl, 10mM HEPES, 20mM tetraethylammonium-Cl, 4mM MgATP, 0.3mM GTP, 0.6mM EGTA, 10mM of QX314 [N-(2,6-dimethylphenyl)carbamoyl-methyl]-triethylammonium bromide] at pH 7.3 and 300 mOsm.

Immunocytochemistry and imaging—Following treatment with either Artemisinins or nocodazole, coverslips were fixed with a 4% PFA, 4% sucrose in PBS at room temperature. Cells were then permeabilized with 0.2% triton-X PBS solution for 30 minutes at room temperature and blocked in 1% bovine serum albumin, 2% goat serum in PBS for 2 hours at room temperature. Next, coverslips were incubated overnight at 4°C with primary antibody diluted in blocking buffer: 1:500 anti-VGAT (131-008, Synaptic Systems), 1:150 anti-gephyrin (147-021, Synaptic Systems), 1:1000 anti-MAP2 (188-006, 188-004 Synaptic Systems), γ 2 1:400 (224-004, Synaptic Systems) and 1:1000 anti- β 3-tubulin (302-302 Synaptic Systems). For γ 2 staining primary antibody incubation was before permeabilization. Following primary antibody incubation coverslips were incubated with a species-appropriate Alexa Fluor secondary antibody for 90 minutes at room temperature. For confocal microscopy, coverslips were mounted on glass slides using aqua-polymont and imaged within the following week. For 3D dSTORM microscopy coverslips did a second fixation step following secondary antibody incubation and stored in PBS.

For confocal images Z-stacks were collected via a Zeiss LSM 710 with 63x objective at 0.1395 μ m/pixel resolution. Synapse density was analyzed using Intellicount (Fantuzzo et al., 2017).

3D dSTORM was performed using Vutara VXL Single Molecule Localization (SML) Super-Resolution Microscope with biplane illumination and a 60x objective. TetraSpeck beads plated on a glass coverslip were used to preform calibration before experiments. Two color imaging was preformed using the 561 nm and 647 nm excitation lasers with 488 nm as the reference channel (MAP2). Samples were imaged in STORM imaging buffer for a maximum of two hours (50 mM tris-HCl (pH 8.0), 10 mM NaCl, 10% glucose, 169 active units glucose oxidase, 1404 active units catalase, 20 mM Cysteamine). All data analysis was performed using Vutara software for single molecule localization, visualization, and statistical analysis. To generate clusters of individual probes DBScan, Density-Based spatial Clustering of Application with Noise, was used with parameters for gephyrin and vGAT clusters: maximum particle distance threshold of 0.1 μ m and minimum particle count threshold of 6 and GABA_AR γ 2 clusters: maximum particle distance threshold of 0.2 μ m and minimum particle count threshold of 6 to calculate cluster surface area and sphericity. Following the identification of gephyrin and vGAT clusters, StormRLA, stochastic optical reconstruction microscopy-based relative localization analysis, was used to compare cluster proximities with a max cluster distance of 1 μ m to define vGAT and gephyrin colocalizing clusters representing a pre- and post-synapse. Once colocalized clusters were determined, cluster volume and cluster centroid distance (distance between the centroids of the pre- and post-synaptic clusters) were calculated. To assess cluster density 5 nm concentrate rings expanding from gephyrin cluster center were created and the number of localizations within each annulus were compared to annulus volume. Pair correlation functions were calculated for individual gephyrin clusters in addition to a theoretical fit to account for cluster density and shape.

RNA extraction, cDNA preparation and qPCR—Following treatment, cells were lysed and RNA extraction was preformed using the PureLink® RNA mini kit with supplementary DNase treatment (Thermo Fisher Scientific) according to manufacturer

protocol. RNA was collected from at least three independent cultures. Extracted RNA was converted to cDNA using the SuperScript® III Reverse Transcriptase kit (Thermo Fisher Scientific) according to manufacturer protocol. RNA was incubated with 1x random primer and 10mM dNTPs at 65°C for 5 minutes. 5x First Strand Buffer, 100mM DTT, RNase out, and SuperScript® III Reverse Transcriptase were then added to the reaction and incubated at 25°C for 5 minutes, 50°C for 1 hour, then 70°C for 15 minutes.

Prepared cDNA was used for qPCR. Reaction mixture: 10 µL of Power SYBR® Green PCR Master Mix (Thermo Fisher Scientific), 7 µL of nuclease-free H₂O, 1 µL of forward primer (10µM), 1 µL of reverse primer (10µM), and 1.5µL of cDNA. Primers: *Gapdh* Forward AGGTCGGTGTGAACGGATTTG, *Gapdh* Reverse TGTAGACCATGTAGTTGAGGTCA, *Bdnf* Forward AGACATGTTTGCGGCATCCAG, *Bdnf* Reverse: CCATAAGGACGCGGACTTGTACA. The qPCR reaction was done in duplicate for each sample with a 2 plateau thermal profile of (1) 50°C for 10 minutes, (2) 95°C for 2 minutes, (3) 95°C for 15 s, (4) 60°C for 1 minute, steps 3–4 were repeated for 40 cycles. All Ct values were normalized to *Gapdh* and analyzed relative to a standard curve.

QUANTIFICATION AND STATISTICAL ANALYSIS

Data presented as mean \pm standard error of mean (SEM). Sample size details are included in figure captions. Sample sizes were based on previous studies performed in our lab as well as in the field of molecular & cellular neuroscience. To quantify tonic inhibition, we calculated the distribution of current around the mean and fit it to a Gaussian distribution to determine the standard deviation. Currents traces were taken at two time points in the beginning of each recording and at two time points after the perfusion of TPMPA. Due to the low frequency of mIPSCs 30 second traces at the same timepoints were selected across all recordings regardless of the presence of a mIPSC. Each set of experiments was performed at least twice with two different sets of neuronal cultures if appropriate. Prism 8 (GraphPad) was used to run all statistical tests including a test of normality was conducted for each data set analyzed, outliers were identified with Robust regression and Outlier removal (ROUT) method, and the appropriate parametric or nonparametric test conducted to compare groups. All statistical details are stated in the figure legends. A $p < 0.05$ was considered as statistically significant.

Supplementary Material

Refer to Web version on PubMed Central for supplementary material.

ACKNOWLEDGMENTS

We would like to thank Dr. Natali Chanaday for her assistance in dSTORM image analysis, writing the MATLAB script for the denoising of mIPSCs, and general experimental advice, and Dr. Baris Alten for his guidance in experimental techniques. We also thank Dr. Patricia Horvath for her insightful comments on the manuscript. This work was supported by the National Institute of Mental Health (grant MH066198 to E.T.K. and T32 MH064913 to N.J.G.). Figures 1A, 1B, 6A, and 7O were created with BioRender.com.

REFERENCES

- Allred MJ, Mulder-Rosi J, Lingenfelter SE, Chen G, and Lüscher B (2005). Distinct gamma2 subunit domains mediate clustering and synaptic function of postsynaptic GABAA receptors and gephyrin. *J. Neurosci* 25, 594–603. 10.1523/JNEUROSCI.4011-04.2005. [PubMed: 15659595]
- Andreae LC, and Burrone J (2018). The role of spontaneous neurotransmission in synapse and circuit development. *J. Neurosci. Res* 96, 354–359. 10.1002/jnr.24154. [PubMed: 29034487]
- Atasoy D, Ertunc M, Moulder KL, Blackwell J, Chung C, Su J, and Kavalali ET (2008). Spontaneous and evoked glutamate release activates two populations of NMDA receptors with limited overlap. *J. Neurosci* 28, 10151–10166. 10.1523/JNEUROSCI.2432-08.2008. [PubMed: 18829973]
- Biederer T, Kaeser PS, and Blanpied TA (2017). Transcellular nanoalignment of synaptic function. *Neuron* 96, 680–696. 10.1016/j.neuron.2017.10.006. [PubMed: 29096080]
- Brady ML, and Jacob TC (2015). Synaptic localization of $\alpha 5$ GABA (A) receptors via gephyrin interaction regulates dendritic outgrowth and spine maturation. *Dev. Neurobiol* 75, 1241–1251. 10.1002/dneu.22280. [PubMed: 25663431]
- Chanaday N (2018). Single-vesicle-fusion-events (GitHub). <https://github.com/nchanaday/Single-vesicle-fusion-events>.
- Chanaday NL, and Kavalali ET (2018). Optical detection of three modes of endocytosis at hippocampal synapses. *Elife* 7, e36097. 10.7554/eLife.36097. [PubMed: 29683423]
- Chen J-C, Lo Y-F, Lin S-H, Huang C-L, and Cheng C-J (2019). WNK4 kinase is a physiological intracellular chloride sensor. *Proc. Natl. Acad. Sci. USA* 116, 4502–4507. [PubMed: 30765526]
- Choi G, and Ko J (2015). Gephyrin: a central GABAergic synapse organizer. *Exp. Mol. Med* 47, e158. 10.1038/emm.2015.5. [PubMed: 25882190]
- Chung SH, and Kennedy RA (1991). Forward-backward non-linear filtering technique for extracting small biological signals from noise. *J. Neurosci. Methods* 40, 71–86. 10.1016/0165-0270(91)90118-j. [PubMed: 1795554]
- Craig AM, Banker G, Chang W, McGrath ME, and Serpinskaya AS (1996). Clustering of gephyrin at GABAergic but not glutamatergic synapses in cultured rat hippocampal neurons. *J. Neurosci* 16, 3166–3177. [PubMed: 8627355]
- Crosby KC, Gookin SE, Garcia JD, Hahn KM, Dell'Acqua ML, and Smith KR (2019). Nanoscale subsynaptic domains underlie the organization of the inhibitory synapse. *Cell Rep.* 26, 3284–3297.e3. 10.1016/j.celrep.2019.02.070. [PubMed: 30893601]
- Essrich C, Lorez M, Benson JA, Fritschy JM, and Lüscher B (1998). Postsynaptic clustering of major GABAA receptor subtypes requires the gamma 2 subunit and gephyrin. *Nat. Neurosci* 1, 563–571. 10.1038/2798. [PubMed: 10196563]
- Fantuzzo JA, Mirabella VR, Hamod AH, Hart RP, Zahn JD, and Pang ZP (2017). Intellicount: high-throughput quantification of fluorescent synaptic protein puncta by machine learning. *ENeuro* 4. 10.1523/ENEURO.0219-17.2017.
- Farrant M, and Nusser Z (2005). Variations on an inhibitory theme: phasic and tonic activation of GABAA receptors. *Nat. Rev. Neurosci* 6, 215–229. 10.1038/nrn1625. [PubMed: 15738957]
- Gonzalez-Islas C, Bülow P, and Wenner P (2018). Regulation of synaptic scaling by action potential-independent miniature neurotransmission. *J. Neurosci. Res* 96, 348–353. 10.1002/jnr.24138. [PubMed: 28782263]
- Guzikowski NJ, and Kavalali ET (2021). Nano-organization at the synapse: segregation of distinct forms of neurotransmission. *Front. Synaptic Neurosci* 13, 796498. [PubMed: 35002671]
- Hartley JM, Chu T-W, Peterson EM, Zhang R, Yang J, Harris J, and Kopeček J (2015). Super-resolution imaging and quantitative analysis of membrane protein/lipid raft clustering mediated by cell-surface self-assembly of hybrid nanoconjugates. *Chembiochem* 16, 1725–1729. 10.1002/cbic.201500278. [PubMed: 26097072]
- Hausrat TJ, Muhia M, Gerrow K, Thomas P, Hirdes W, Tsukita S, Heisler FF, Herich L, Dubroqua S, Breiden P, et al. (2015). Radixin regulates synaptic GABAA receptor density and is essential for reversal learning and short-term memory. *Nat. Commun* 6, 6872. 10.1038/ncomms7872. [PubMed: 25891999]

- Heubl M, Zhang J, Pressey JC, Al Awabdh S, Renner M, Gomez-Castro F, Moutkine I, Eugène E, Rousseau M, Kahle KT, et al. (2017). GABA A receptor dependent synaptic inhibition rapidly tunes KCC2 activity via the Cl⁻-sensitive WNK1 kinase. *Nat. Commun* 8, 1776. 10.1038/s41467-017-01749-0. [PubMed: 29176664]
- Horvath PM, Piazza MK, Monteggia LM, and Kavalali ET (2020). Spontaneous and evoked neurotransmission are partially segregated at inhibitory synapses. *Elife* 9, e52852. 10.7554/eLife.52852. [PubMed: 32401197]
- Horvath PM, Chanaday NL, Alten B, Kavalali ET, and Monteggia LM (2021). A subthreshold synaptic mechanism regulating BDNF expression and resting synaptic strength. *Cell Rep.* 36, 109467. 10.1016/j.celrep.2021.109467. [PubMed: 34348149]
- Jacob TC, Bogdanov YD, Magnus C, Saliba RS, Kittler JT, Haydon PG, and Moss SJ (2005). Gephyrin regulates the cell surface dynamics of synaptic GABAA receptors. *J. Neurosci* 25, 10469–10478. 10.1523/JNEUROSCI.2267-05.2005. [PubMed: 16280585]
- Kasaragod VB, Hausrat TJ, Schaefer N, Kuhn M, Christensen NR, Tessmer I, Maric HM, Madsen KL, Sotriffer C, Villmann C, et al. (2019). Elucidating the molecular basis for inhibitory neurotransmission regulation by artemisinin. *Neuron* 101, 673–689.e11. 10.1016/j.neuron.2019.01.001. [PubMed: 30704910]
- Kavalali ET (2018). Spontaneous neurotransmission: a form of neural communication comes of age. *J. Neurosci. Res* 96, 331–334. 10.1002/jnr.24207. [PubMed: 29219198]
- Kavalali ET, Klingauf J, and Tsien RW (1999). Activity-dependent regulation of synaptic clustering in a hippocampal culture system. *Proc. Natl. Acad. Sci. USA* 96, 12893–12900. 10.1073/pnas.96.22.12893. [PubMed: 10536019]
- Kirsch J, and Betz H (1995). The postsynaptic localization of the glycine receptor-associated protein gephyrin is regulated by the cytoskeleton. *J. Neurosci* 15, 4148–156. 10.1523/JNEUROSCI.15-06-04148.1995. [PubMed: 7790902]
- Kirsch J, Langosch D, Prior P, Littauer UZ, Schmitt B, and Betz H (1991). The 93-kDa glycine receptor-associated protein binds to tubulin. *J. Biol. Chem* 266, 22242–22245. [PubMed: 1657993]
- Kneussel M, Brandstätter JH, Laube B, Stahl S, Müller U, and Betz H (1999). Loss of postsynaptic GABA(A) receptor clustering in gephyrin-deficient mice. *J. Neurosci* 19, 9289–9297. [PubMed: 10531433]
- Kneussel M, Brandstätter JH, Gasnier B, Feng G, Sanes JR, and Betz H (2001). Gephyrin-independent clustering of postsynaptic GABA(A) receptor subtypes. *Mol. Cell. Neurosci* 17, 973–982. 10.1006/mcne.2001.0983. [PubMed: 11414787]
- Kusick GF, Chin M, Raychaudhuri S, Lippmann K, Adula KP, Hujber EJ, Vu T, Davis MW, Jorgensen EM, and Watanabe S (2020). Synaptic vesicles transiently dock to refill release sites. *Nat. Neurosci* 23, 1329–1338. 10.1038/s41593-020-00716-1. [PubMed: 32989294]
- Lévi S, Logan SM, Tovar KR, and Craig AM (2004). Gephyrin is critical for Glycine receptor clustering but not for the formation of functional GABAergic synapses in hippocampal neurons. *J. Neurosci* 24, 207–217. 10.1523/JNEUROSCI.1661-03.2004. [PubMed: 14715953]
- Li J, Casteels T, Frogne T, Ingvorsen C, Honoré C, Courtney M, Huber KVM, Schmitner N, Kimmel RA, Romanov RA, et al. (2017). Artemisinin target GABAA receptor signaling and impair α cell identity. *Cell* 168, 86–100.e15. 10.1016/j.cell.2016.11.010. [PubMed: 27916275]
- Li S, Raychaudhuri S, Lee SA, Brockmann MM, Wang J, Kusick G, Prater C, Syed S, Falahati H, Ramos R, et al. (2021). Asynchronous release sites align with NMDA receptors in mouse hippocampal synapses. *Nat. Commun* 12, 677. 10.1038/s41467-021-21004-x. [PubMed: 33514725]
- Ligon LA, and Steward O (2000). Role of microtubules and actin filaments in the movement of mitochondria in the axons and dendrites of cultured hippocampal neurons. *J. Comp. Neurol* 427, 351–361. 10.1002/1096-9861(20001120)427:3<351::AID-CNE3>3.0.CO;2-R. [PubMed: 11054698]
- Liu Y-T, Tao C-L, Zhang X, Xia W, Shi D-Q, Qi L, Xu C, Sun R, Li X-W, Lau P-M, et al. (2020). Mesophasic organization of GABA A receptors in hippocampal inhibitory synapses. *Nat. Neurosci* 23, 1589–1596. 10.1038/s41593-020-00729-w. [PubMed: 33139942]

- Maric H-M, Mukherjee J, Tretter V, Moss SJ, and Schindelin H (2011). Gephyrin-mediated γ -aminobutyric acid type A and glycine receptor clustering relies on a common binding site. *J. Biol. Chem* 286, 42105–42114. 10.1074/jbc.M111.303412. [PubMed: 22006921]
- Maric HM, Hausrat TJ, Neubert F, Dalby NO, Doose S, Sauer M, Kneussel M, and Strømgaard K (2017). Gephyrin-binding peptides visualize postsynaptic sites and modulate neurotransmission. *Nat. Chem. Biol* 13, 153–160. 10.1038/nchembio.2246. [PubMed: 27893705]
- Maschi D, and Klyachko VA (2017). Spatiotemporal regulation of synaptic vesicle fusion sites in central synapses. *Neuron* 94, 65–73.e3. 10.1016/j.neuron.2017.03.006. [PubMed: 28343869]
- Meier J, Vannier C, Sergé A, Triller A, and Choquet D (2001). Fast and reversible trapping of surface glycine receptors by gephyrin. *Nat. Neurosci* 4, 253–260. 10.1038/85099. [PubMed: 11224541]
- Melom JE, Akbergenova Y, Gavornik JP, and Littleton JT (2013). Spontaneous and evoked release are independently regulated at individual active zones. *J. Neurosci* 33, 17253–17263. 10.1523/JNEUROSCI.3334-13.2013. [PubMed: 24174659]
- Meyer DK, Olenik C, Hofmann F, Barth H, Leemhuis J, Brünig I, Aktories K, and Nörenberg W (2000). Regulation of somatodendritic GABAA receptor channels in rat hippocampal neurons: evidence for a role of the small GTPase Rac1. *J. Neurosci* 20, 6743–6751. 10.1523/JNEUROSCI.20-18-06743.2000. [PubMed: 10995817]
- Peled ES, Newman ZL, and Isacoff EY (2014). Evoked and spontaneous transmission favored by distinct sets of synapses. *Curr. Biol* 24, 484–493. 10.1016/j.cub.2014.01.022. [PubMed: 24560571]
- Pennacchietti F, Vascon S, Nieuw T, Rosillo C, Das S, Tyagarajan SK, Diaspro A, Del Bue A, Petrini EM, Barberis A, et al. (2017). Nanoscale molecular reorganization of the inhibitory postsynaptic density is a determinant of GABAergic synaptic potentiation. *J. Neurosci* 37, 1747–1756. 10.1523/JNEUROSCI.0514-16.2016. [PubMed: 28073939]
- Piala AT, Moon TM, Akella R, He H, Cobb MH, and Goldsmith EJ (2014). Chloride sensing by WNK1 involves inhibition of autophosphorylation. *Sci. Signal* 7, ra41. [PubMed: 24803536]
- Ramsey AM, Tang A-H, LeGates TA, Gou X-Z, Carbone BE, Thompson SM, Biederer T, and Blanpied TA (2021). Subsynaptic positioning of AMPARs by LRRTM2 controls synaptic strength. *Sci. Adv* 7, eabf3126. 10.1126/sciadv.abf3126. [PubMed: 34417170]
- Reese AL, and Kavalali ET (2016). Single synapse evaluation of the post-synaptic NMDA receptors targeted by evoked and spontaneous neurotransmission. *Elife* 5, e21170. 10.7554/eLife.21170. [PubMed: 27882871]
- Sara Y, Bal M, Adachi M, Monteggia LM, and Kavalali ET (2011). Use-dependent AMPA receptor block reveals segregation of spontaneous and evoked glutamatergic neurotransmission. *J. Neurosci* 31, 5378–5382. 10.1523/JNEUROSCI.5234-10.2011. [PubMed: 21471372]
- Sassò-Pognetto M, Panzanelli P, Sieghart W, and Fritschy JM (2000). Colocalization of multiple GABA(A) receptor subtypes with gephyrin at post-synaptic sites. *J. Comp. Neurol* 420, 481–498. 10.1002/(sici)1096-9861. [PubMed: 10805922]
- Sassò-Pognetto M, Frola E, Pregno G, Briatore F, and Patrizi A (2011). Understanding the molecular diversity of GABAergic synapses. *Front. Cell. Neurosci* 5, 4. 10.3389/fncel.2011.00004. [PubMed: 21713106]
- Sengupta P, Jovanovic-Taliman T, and Lippincott-Schwartz J (2013). Quantifying spatial organization in point-localization superresolution images using pair correlation analysis. *Nat. Protoc* 8, 345–354. 10.1038/nprot.2013.005. [PubMed: 23348362]
- Sperk G, Schwarzer C, Tsunashima K, Fuchs K, and Sieghart W (1997). GABAA receptor subunits in the rat hippocampus I: immunocytochemical distribution of 13 subunits. *Neuroscience* 80, 987–1000. 10.1016/S0306-4522(97)00146-2. [PubMed: 9284055]
- Tang A-H, Chen H, Li TP, Metzbower SR, MacGillavry HD, and Blanpied TA (2016). A trans-synaptic nanocolumn aligns neurotransmitter release to receptors. *Nature* 536, 210–214. 10.1038/nature19058. [PubMed: 27462810]
- Thomas P, Mortensen M, Hosie AM, and Smart TG (2005). Dynamic mobility of functional GABA A receptors at inhibitory synapses. *Nat. Neurosci* 8, 889–897. 10.1038/nn1483. [PubMed: 15951809]
- Tu Y (2016). Artemisinin—a gift from traditional Chinese medicine to the world (nobel lecture). *Angew. Chem. Int. Ed. Engl* 55, 10210–10226. 10.1002/anie.201601967. [PubMed: 27488942]

- Vaden RJ, Gonzalez JC, Tsai M-C, Niver AJ, Fusilier AR, Griffith CM, Kramer RH, Wadiche JI, and Overstreet-Wadiche L (2020). Parvalbumin interneurons provide spillover to newborn and mature dentate granule cells. *Elife* 9, e54125. 10.7554/eLife.54125. [PubMed: 32602839]
- Yu W, Jiang M, Miralles CP, Li RW, Chen G, and de Blas AL (2007). Gephyrin clustering is required for the stability of GABAergic synapses. *Mol. Cell. Neurosci* 36, 484–500. 10.1016/j.mcn.2007.08.008. [PubMed: 17916433]
- van Zundert B, Castro P, and Aguayo LG (2005). Glycinergic and GABAergic synaptic transmission are differentially affected by gephyrin in spinal neurons. *Brain Res.* 1050, 40–47. 10.1016/j.brainres.2005.05.014. [PubMed: 15963957]

Author Manuscript

Author Manuscript

Author Manuscript

Author Manuscript

Highlights

- Gephyrin mediates nano-segregation of spontaneous and evoked neurotransmission
- Clustering dynamics of GABA_AR γ 2 subunits parallel gephyrin cluster size and density
- Evoked and spontaneous GABAergic neurotransmission show center-surround organization
- GABAergic spontaneous neurotransmission regulates *Bdnf* expression

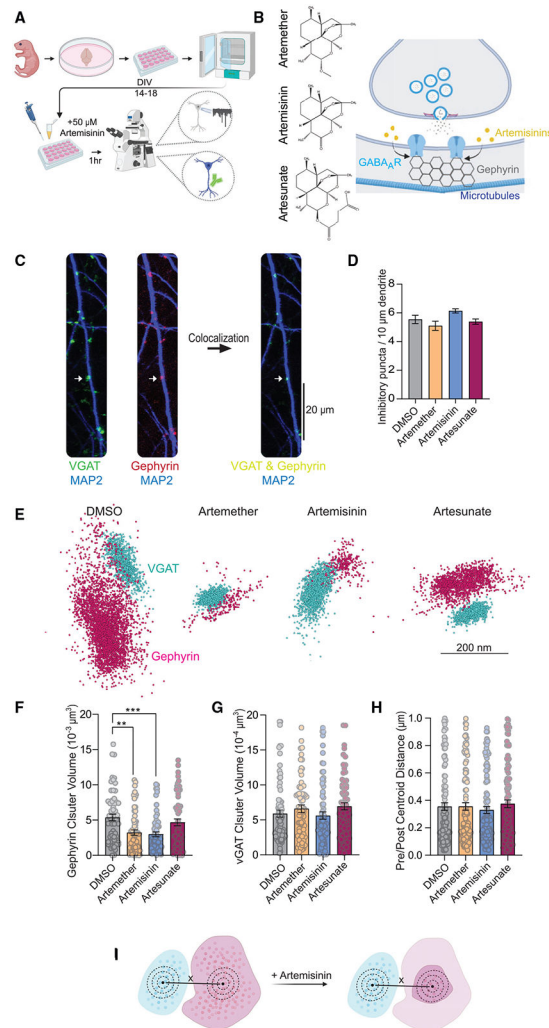


Figure 1. Artemisinin treatment has a specific postsynaptic effect, decreasing gephyrin cluster volume

(A) Description of experimental design; preparation of primary hippocampal cultures and treatment with artemisinins before electrophysiology and immunocytochemistry experiments.

(B) Molecular structure of artemisinins (Kasaragod et al., 2019) and diagram of molecular interaction of artemisinins and GABA_AR intracellular loops between transmembrane domains 3–4 binding to the gephyrin universal binding pocket on the GephE domain.

(C) Following 1-h control (DMSO) and 50 μM artemisinin treatment, neurons were co-immunolabeled for vGAT (presynaptic marker, green), gephyrin (postsynaptic marker, red), and MAP2 (dendrite, blue). The colocalization of vGAT and gephyrin puncta represent inhibitory puncta.

(D) Quantitative analyses of inhibitory puncta per 10 μm of dendrite (ordinary one-way ANOVA $p = 0.0137$, Dunnett's multiple comparisons test DMSO versus artemether $p = 0.4367$, DMSO versus artemisinin $p = 0.1475$, DMSO versus artesunate $p = 0.9308$. Sample size is equivalent to number of regions imaged: DMSO $n = 12$, artemether $n = 10$, artemisinin $n = 16$, artesunate $n = 13$).

(E) 3D dSTORM reconstructions of colocalized and pre- and postsynaptic clusters with localizations color coded by probe (vGAT, blue; gephyrin, pink).

(F) Quantitative analyses of gephyrin cluster volume (Kruskal-Wallis test $p = 0.0001$, Dunn's multiple comparisons test DMSO versus artemether $p = 0.0011$, DMSO versus artemisinin $p = 0.0003$, DMSO versus artesunate $p = 0.4738$. Sample size is equivalent to number of regions imaged: DMSO $n = 7$, artemether $n = 7$, artemisinin $n = 9$, artesunate $n = 6$).

(G) vGAT cluster volume (Kruskal-Wallis test $p = 0.0872$, Dunn's multiple comparisons test DMSO versus artemether $p = 0.9122$, DMSO versus artemisinin $p > 0.9999$, DMSO versus artesunate $p = 0.19991$. Sample size is equivalent to number of regions imaged: DMSO $n = 7$, artemether $n = 7$, artemisinin $n = 9$, artesunate $n = 6$).

(H) Distance between center of vGAT and gephyrin colocalized clusters (Kruskal-Wallis test $p = 0.8732$, Dunn's multiple comparisons DMSO versus artemether $p > 0.9999$, DMSO versus artemisinin $p > 0.9999$, DMSO versus artesunate $p > 0.9999$. Sample size is equivalent to number of regions imaged: DMSO $n = 7$, artemether $n = 7$, artemisinin $n = 9$, artesunate $n = 6$).

(I) Proposed schematic of how pre- and postsynapse centroid distance is unchanged following the loss of gephyrin. Graphs are mean \pm SEM. Significance reported as * $p < 0.05$, ** $p < 0.01$, *** $p < 0.001$, and **** $p < 0.0001$. NS denotes non-significance.

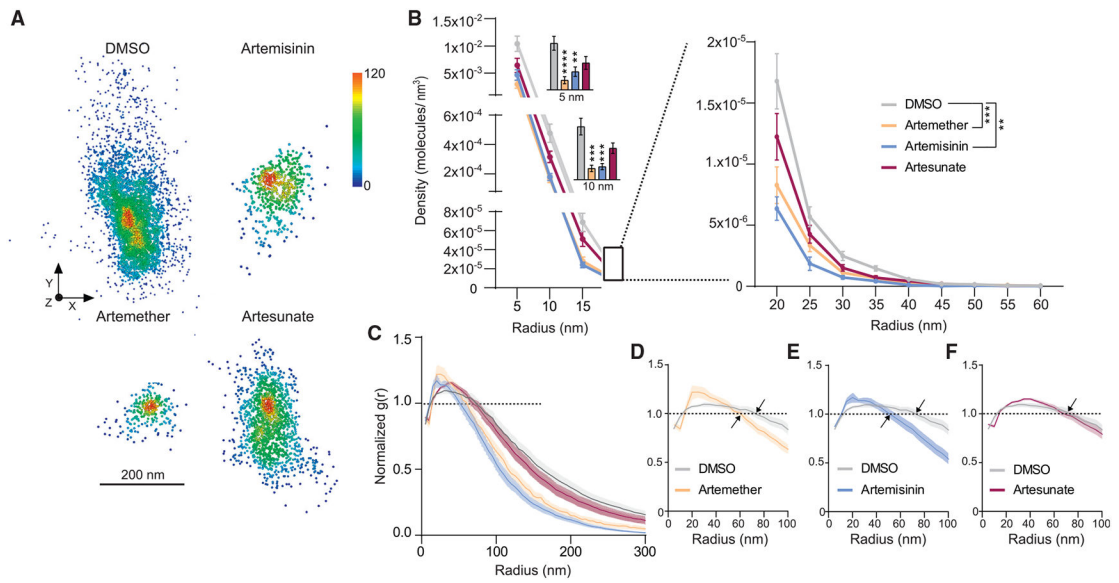
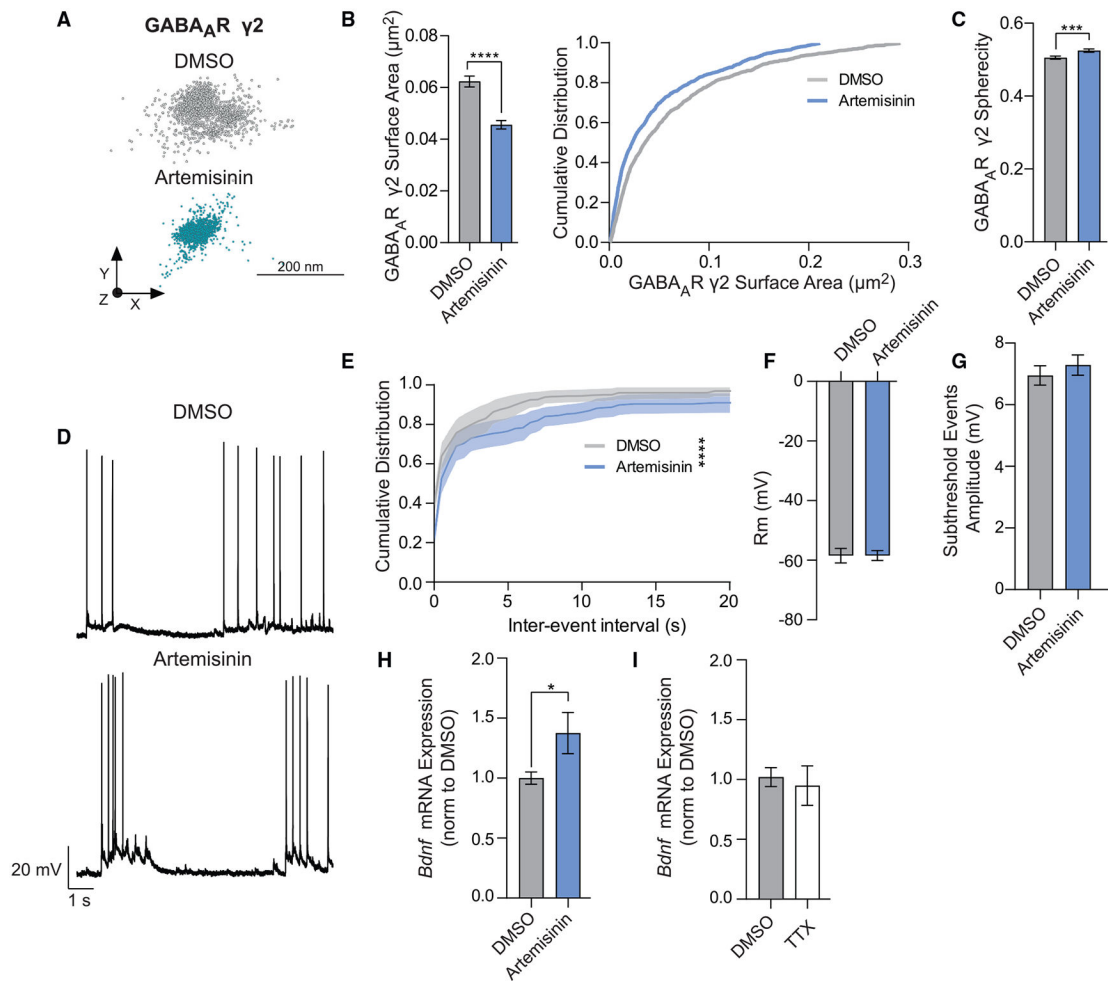


Figure 2. Artemether and parental artemisinin decrease gephyrin cluster density

(A) 3D dSTORM reconstructions of gephyrin molecules with localizations represented by density heatmap.

(B) Quantitative analysis of gephyrin cluster density at individual annuli thickness of 5 nm (mixed-effects analysis treatment group factor $p < 0.0001$, DMSO versus artemether $p = 0.0002$, DMSO versus artemisinin $p = 0.0024$, DMSO versus artesunate $p = 0.1558$. Sample size is equivalent to number of clusters analyzed: DMSO $n = 35$, artemether $n = 31$, artemisinin $n = 34$, artesunate $n = 35$; refer to Table S1 for individual radii statistical results).

(C–F) (C) Pair correlation functions of gephyrin clusters for all treatment groups to a radius of 300 nm and (D) for artemether ($n = 28$) and DMSO ($n = 34$) to 100 nm radius, (E) artemisinin ($n = 33$) and DMSO to 100 nm radius, and (F) artesunate ($n = 33$) and DMSO to 100 nm radius. Graphs are mean \pm SEM. Significance reported as * $p < 0.05$, ** $p < 0.01$, *** $p < 0.001$, and **** $p < 0.0001$. NS denotes non-significance.



(H) *Bdnf* mRNA expression normalized to DMSO following artemisinin (unpaired t test, $p = 0.0343$, sample size is equivalent to the number of independent groups: DMSO $n = 10$, artemisinin $n = 8$).

(I) Tetrodotoxin (TTX) treatment (unpaired t test, $p = 0.7890$, DMSO $n = 6$, TTX $n = 6$). Graphs are mean \pm SEM. Significance reported as * $p < 0.05$, ** $p < 0.01$, *** $p < 0.001$, and **** $p < 0.0001$. NS denotes non-significance.

Author Manuscript

Author Manuscript

Author Manuscript

Author Manuscript

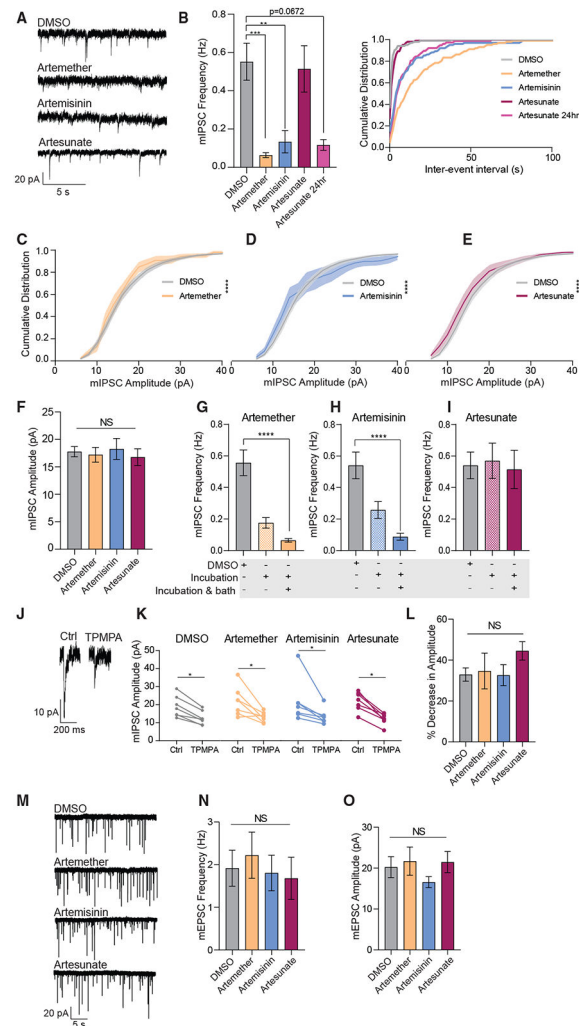


Figure 4. Artemether and parental artemisinin treatment selectivity decreased inhibitory miniature events

(A) Representative traces of whole-cell voltage-clamp mIPSCs following 1-h control (DMSO) and 50 μ M artemisinin treatment.

(B) Quantitative analyses of mIPSC frequency (Kruskal-Wallis test $p < 0.0001$, Dunn's multiple comparisons test DMSO versus artemether $p = 0.0002$, DMSO versus artemisinin $p = 0.0020$, DMSO versus artesunate $p > 0.9999$, DMSO versus artesunate 24 h $p = 0.0672$. Sample size is equivalent to number of cells recorded from DMSO: $n = 15$, artemether $n = 8$, artemisinin $n = 10$, artesunate $n = 12$, artesunate 24 h $n = 5$) and cumulative distribution of mIPSC inter-event intervals (IEIs).

(C) Cumulative distribution of mIPSC amplitude following artemether treatment (Kolmogorov-Smirnov test $p < 0.0001$, DMSO $n = 15$, artemether $n = 8$).

(D) Artemisinin treatment (Kolmogorov-Smirnov test $p < 0.0001$, DMSO $n = 15$, artemisinin $n = 10$).

(E) Artesunate treatment (Kolmogorov-Smirnov test $p < 0.0001$, DMSO $n = 15$, artesunate $n = 12$).

- (F) Quantitative analysis of mIPSC amplitude (average per coverslip) (ordinary one-way ANOVA $p = 0.2030$. Sample size is equivalent to number of cells recorded from DMSO $n = 15$, artemether $n = 8$, artemisinin $n = 10$, artesunate $n = 12$).
- (G) Quantitative analyses of mIPSC frequency following 1-h control (DMSO) and 50 μM artemether treatment with artemether included (same data as Figure 4B) and not included in Tyrode's bath solution (Kruskal-Wallis test, $p < 0.0001$, Dunn's multiple comparison test DMSO versus artemether incubation $p = 0.1035$, DMSO versus artemether incubation + bath $p < 0.0001$, artemether incubation versus artemether incubation + bath $p = 0.2954$, DMSO $n = 17$, artemether incubation $n = 6$, artemether incubation + bath $n = 10$).
- (H) 50 μM artemisinin treatment with artemisinin included (same data as Figure 4B) and not included in Tyrode's bath solution (Kruskal-Wallis test, $p < 0.0001$, Dunn's multiple comparison test DMSO versus artemisinin incubation $p = 0.3020$, DMSO versus artemisinin incubation + bath $p < 0.0001$, artemisinin incubation versus artemisinin incubation + bath $p = 0.0506$, DMSO $n = 18$, artemisinin incubation $n = 9$, artemisinin incubation + bath $n = 12$).
- (I) 50 μM artesunate treatment with artesunate included (same data as Figure 4B) and not included in Tyrode's bath solution (Kruskal-Wallis test, $p = 0.6794$, Dunn's multiple comparison test DMSO versus artesunate incubation $p > 0.999$, DMSO versus artemisinin incubation + bath $p > 0.999$, artesunate incubation versus artesunate incubation + bath $p > 0.999$, DMSO $n = 17$, artesunate incubation $n = 8$, artesunate incubation + bath $n = 12$).
- (J) Representative traces of mIPSC peaks in control (DMSO) treatment at baseline and following 200 μM TPMPA perfusion.
- (K) Quantitative analyses of decrease in mIPSC amplitude following TPMPA perfusion (Wilcoxon matched-pairs signed rank test DMSO $p = 0.0156$, artemether $p = 0.0313$, artemisinin $p = 0.0156$, artesunate $p = 0.0156$. Sample size is equivalent to number of cells recorded from DMSO $n = 7$, artemether $n = 7$, artemisinin $n = 7$, artesunate $n = 7$).
- (L) Quantitative analyses of percentage decrease in mIPSC amplitude following TPMPA perfusion (Kruskal-Wallis test, $p = 0.3321$, Dunn's multiple comparison test DMSO versus artemether $p > 0.9999$, DMSO versus artemisinin $p > 0.9999$, DMSO versus artesunate $p = 0.3342$. Sample size is equivalent to number of cells recorded from DMSO $n = 7$, artemether $n = 7$, artemisinin $n = 7$, artesunate $n = 7$).
- (M) Representative traces of whole-cell voltage-clamp mEPSCs following 1-h control (DMSO) and 50 μM artemisinin treatment.
- (N and O) (N) Quantitative analyses of mEPSC frequency (Kruskal-Wallis test, $p = 0.6979$, Dunn's multiple comparison test DMSO versus artemether $p > 0.9999$, DMSO versus artemisinin $p > 0.9999$, DMSO versus artesunate $p > 0.9999$. Sample size is equivalent to number of cells recorded from DMSO $n = 11$, artemether $n = 11$, artemisinin $n = 15$, artesunate $n = 14$) and (O) mEPSC amplitude (Kruskal-Wallis test, $p = 0.7366$, Dunn's multiple comparison test DMSO versus artemether $p > 0.9999$, DMSO versus artemisinin $p > 0.9999$, DMSO versus artesunate $p > 0.9999$. Sample size is equivalent to number of cells recorded from DMSO $n = 11$, artemether $n = 11$, artemisinin $n = 15$, artesunate $n = 14$).
- Graphs are mean \pm SEM. Significance reported as * $p < 0.05$, ** $p < 0.01$, *** $p < 0.001$, and **** $p < 0.0001$. NS denotes non-significance.

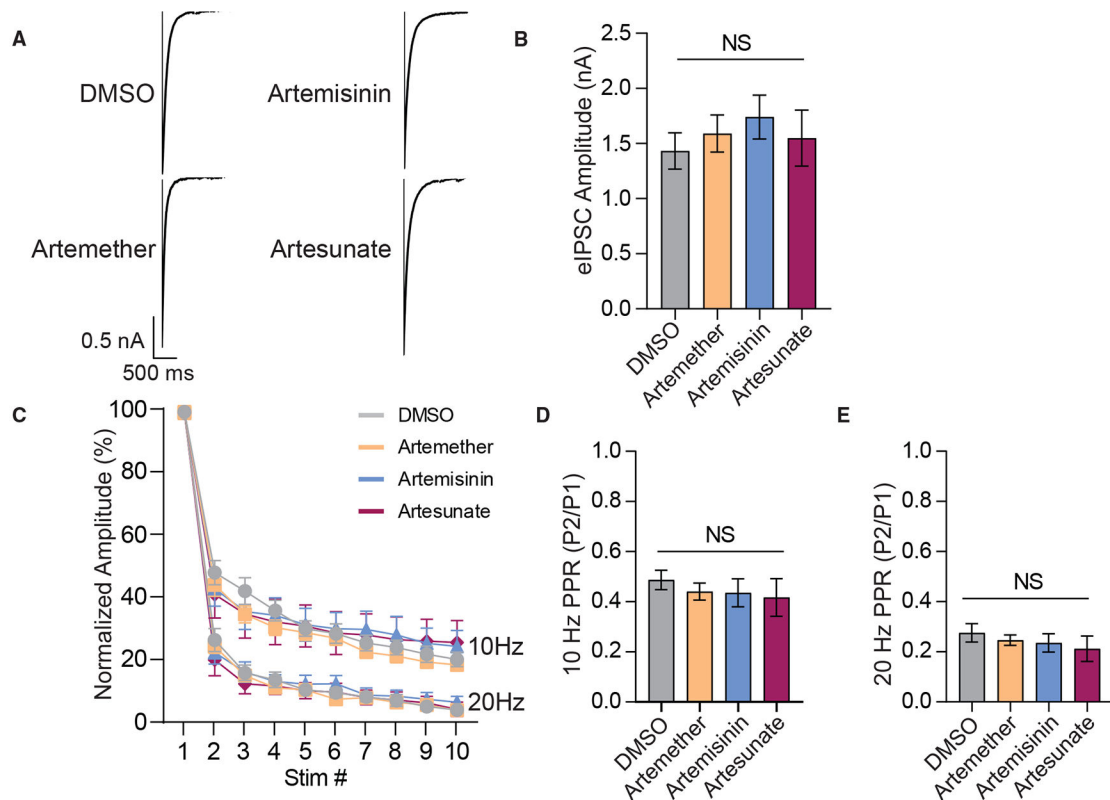


Figure 5. Artemisinin treatment did not alter eIPSC amplitude

(A) Representative traces of whole-cell voltage-clamp eIPSCs following 1-h control (DMSO) and 50 μ M artemisinin treatment.

(B) Quantitative analyses of eIPSC amplitude (ordinary one-way ANOVA $p = 0.6983$, Dunnett's multiple comparisons test DMSO versus artemether $p = 0.8745$, DMSO versus artemisinin $p = 0.5277$, DMSO versus artesunate $p = 0.9591$. Sample size is equivalent to number of cells recorded from DMSO $n = 18$, artemether $n = 13$, artemisinin $n = 11$, artesunate $n = 9$).

(C) Ten stimulations at 10 Hz and 20 Hz were applied to each group with the quantification of paired pulse ratio using the amplitude of the postsynaptic current of the first and second stimulation.

(D) 10 Hz (ordinary one-way ANOVA $p = 0.7246$, Dunnett's multiple comparisons test DMSO versus artemether $p = 0.8258$, DMSO versus artemisinin $p = 0.8064$, DMSO versus artesunate $p = 0.6556$, DMSO $n = 20$, artemether $n = 12$, artemisinin $n = 10$, artesunate $n = 9$).

(E) 20 Hz (Kruskal-Wallis test, $p = 0.7560$, Dunn's multiple comparison test DMSO versus artemether $p > 0.9999$, DMSO versus artemisinin $p > 0.9999$, DMSO versus artesunate $p = 0.9917$. Sample size is equivalent to number of cells recorded from DMSO $n = 19$, artemether $n = 12$, artemisinin $n = 10$, artesunate $n = 7$). Graphs are mean \pm SEM. Significance reported as * $p < 0.05$, ** $p < 0.01$, *** $p < 0.001$, and **** $p < 0.0001$. NS denotes non-significance.

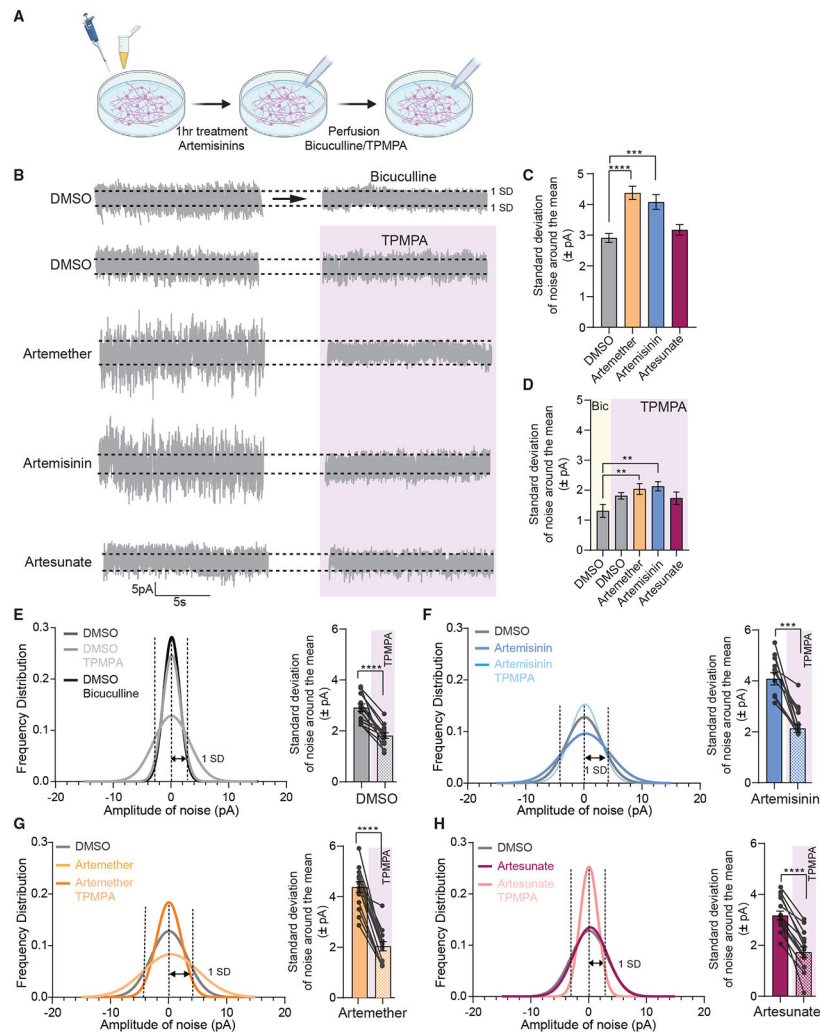


Figure 6. Artemisinin treatment augments tonic inhibition

(A) Description of experimental design: 1-h treatment with artemisinins followed by baseline and bicuculline/TPMPA post-perfusion electrophysiology experiments.

(B) Representative traces of tonic inhibitory current before and after bicuculline or TPMPA perfusion. Black dotted lines are representative of one standard deviation from the mean at baseline.

(C) Tonic inhibitory baseline current was quantified by fitting the distribution of the noise around the mean to a Gaussian curve; a smaller standard deviation translates to a smaller dispersion of noise (ordinary one-way ANOVA $p < 0.0001$, Dunnett's multiple comparisons test DMSO versus artemether $p < 0.0001$, DMSO versus artemisinin $p = 0.0003$, DMSO versus artesunate $p = 0.6731$, DMSO $n = 14$, artemether $n = 14$, artemisinin $n = 14$, artesunate $n = 14$).

(D) The standard deviation of tonic inhibitory current following bicuculline or TPMPA perfusion (Kruskal-Wallis test $p = 0.0018$, Dunn's multiple comparisons test bicuculline versus artemether $p = 0.0076$, bicuculline versus artemisinin $p = 0.0018$; all other comparisons not significant. Sample size is equivalent to number of baseline traces

analyzed: bicuculline n = 14, DMSO n = 14, artemether n = 14, artemisinin n = 14, artesunate n = 14).

(E) Frequency distribution of tonic current around the mean of each group (paired t test DMSO versus DMSO TPMPA $p < 0.0001$).

(F) Frequency distribution of tonic current around the mean of each group (Wilcoxon test artemisinin versus artemisinin TPMPA $p = 0.0001$).

(G) Frequency distribution of tonic current around the mean of each group (paired t test artemether versus artemether TPMPA $p < 0.0001$).

(H) Frequency distribution of tonic current around the mean of each group (paired t test artesunate versus artesunate TPMPA $p < 0.0001$). Graphs are mean \pm SEM. Significance reported as * $p < 0.05$, ** $p < 0.01$, *** $p < 0.001$, and **** $p < 0.0001$. NS denotes non-significance.

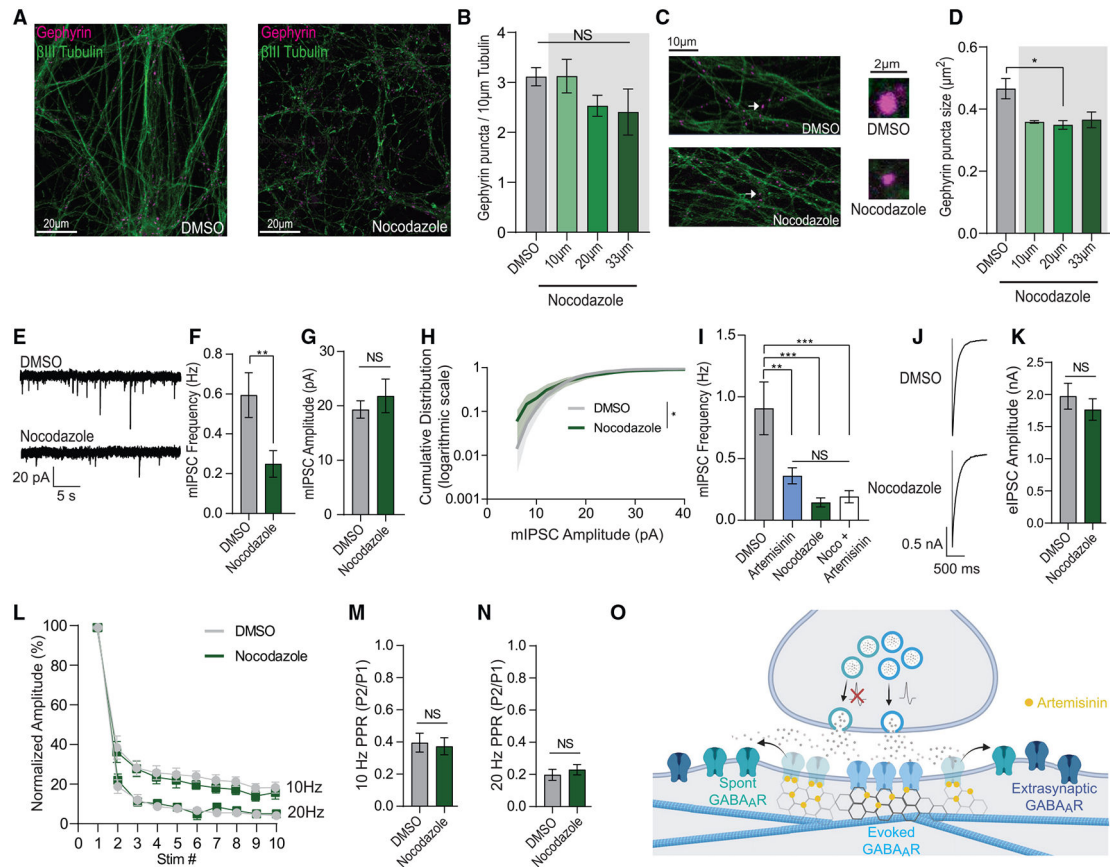


Figure 7. Disruption of microtubule polymerization preferentially affected inhibitory miniature events

(A) Following 1-h control (DMSO) and 33 μ M (10 mg/1 mL) nocodazole treatment, neurons were co-immunolabeled for gephyrin (postsynaptic marker, pink) and β III tubulin (neuronal tubulin, green).

(B) Quantitative analysis of gephyrin puncta per 10 μ m of β III tubulin (Kruskal-Wallis test $p = 0.2535$, Dunn's multiple comparisons test DMSO versus 10 μ M $p > 0.9999$, DMSO versus 20 μ M $p = 0.4111$, DMSO versus 33 μ M $p = 0.3666$. Sample size is equivalent to number of regions imaged: DMSO = 6, 10 μ M = 3, 20 μ M = 5, 33 μ M = 5).

(C) Gephyrin puncta size.

(D) Quantitative analysis of gephyrin puncta size following 1-h treatment with increasing concentrations of nocodazole. (Kruskal-Wallis test $p = 0.0078$, Dunn's multiple comparisons test DMSO versus 10 μ M $p = 0.1204$, DMSO versus 20 μ M $p = 0.0117$, DMSO versus 33 μ M $p = 0.0874$. Sample size is equivalent to number of regions imaged: DMSO = 6, 10 μ M = 3, 20 μ M = 5, 33 μ M = 5).

(E) Representative traces of whole-cell voltage-clamp mIPSCs following 1-h control (DMSO) and 33 μ M nocodazole treatment.

(F and G) (F) Quantitative analysis of mIPSC frequency (Mann-Whitney test DMSO versus nocodazole $p = 0.0097$. Sample size is equivalent to number of cells recorded from DMSO $n = 8$, nocodazole $n = 11$) and (G) mIPSC amplitude (two-tailed unpaired t test DMSO versus

nocodazole $p = 0.5286$. Sample size is equivalent to number of cells recorded from DMSO $n = 8$, nocodazole $n = 11$).

(H) Cumulative distribution of mIPSC amplitude following nocodazole treatment (Kolmogorov-Smirnov test $p = 0.0212$. Sample size is equivalent to number of cells recorded from DMSO $n = 8$, nocodazole $n = 11$).

(I) Analysis of the combined effect of artemisinin and nocodazole treatment on mIPSC frequency (ordinary one-way ANOVA $p < 0.0001$, Tukey's multiple comparisons test DMSO versus artemisinin $p = 0.0052$, DMSO versus nocodazole $p = 0.0002$, DMSO versus artemisinin + nocodazole $p = 0.0006$, artemisinin versus nocodazole $p = 0.5062$, artemisinin versus artemisinin + nocodazole $p = 0.7110$, nocodazole versus artemisinin + nocodazole $p = 0.9922$. Sample size is equivalent to number of cells recorded from DMSO $n = 11$, artemisinin $n = 14$, nocodazole $n = 11$, artemisinin + nocodazole $n = 10$).

(J) Representative traces of eIPSCs following 1-h control (DMSO) and 33 μM nocodazole treatment.

(K) Quantitative analysis of eIPSC amplitude (two-tailed unpaired t test DMSO versus nocodazole $p = 0.4480$. Sample size is equivalent to number of cells recorded from DMSO $n = 12$, nocodazole $n = 10$).

(L) Ten stimulations at 10 Hz and 20 Hz were applied to each group with the quantification of paired pulse ratio using the amplitude of the postsynaptic current of the first and second stimulation.

(M) 10 Hz (two-tailed unpaired t test DMSO versus nocodazole $p = 0.7816$. Sample size is equivalent to number of cells recorded from DMSO $n = 9$, nocodazole $n = 9$).

(N) 20 Hz (Mann-Whitney DMSO versus nocodazole $p = 0.3401$. Sample size is equivalent to number of cells recorded from DMSO $n = 9$, nocodazole $n = 9$).

(O) Proposed schematic of GABA_AR clustering following artemisinin treatment: artemisinin selectively disrupts peripheral GABA_AR clusters mediating spontaneous release, increasing their mobility and the number receptors mediating tonic inhibition, while evoked release is unaffected. Graphs are mean \pm SEM. Significance reported as * $p < 0.05$, ** $p < 0.01$, *** $p < 0.001$, and **** $p < 0.0001$. NS denotes non-significance.

KEY RESOURCES TABLE

REAGENT or RESOURCE	SOURCE	IDENTIFIER
Antibodies		
Anti-Gephyrin (mouse monoclonal)	Synaptic Systems	Cat# 147 021; RRID: AB_2232546
Anti-vGAT (rabbit monoclonal)	Synaptic Systems	Cat# 131 008; RRID: AB_2800534
Anti-MAP2 (chicken polyclonal)	Synaptic Systems	Cat# 188 006 RRID:AB_2619881
Anti-MAP2 (guinea pig polyclonal)	Synaptic Systems	Cat# 188-004 RRID: AB_2138181
Anti- β 3-tubulin (rabbit polyclonal)	Synaptic Systems	Cat# 302-302 RRID: AB_10637424
Anti-GABA _A R- γ 2 (guinea pig polyclonal)	Synaptic Systems	Cat# 224-004 RRID: AB_10594245
Primer: <i>Gapdh</i> Forward AGGTCGGTGTGAACGGATTG	Horvath et al. 2021	N/A
Primer <i>Gapdh</i> Reverse TGTAGACCATGTAGTTGAGGTCA	Horvath et al. 2021	N/A
Primer: <i>Bdnf</i> Forward AGACATGTTTGCGGCATCCAG	Horvath et al. 2021	N/A
Primer: <i>Bdnf</i> Reverse: CCATAAGGACGCGGACTTGTACA	Horvath et al. 2021	N/A
Chemicals, peptides, and recombinant proteins		
6-Cyano-7-nitroquinoxaline-2,3-dione disodium salt hydrate (CNQX)	Sigma-Aldrich	Cat# C239
D(-)-2-Amino-5-phosphonopentanoic acid (AP-5)	Sigma-Aldrich	Cat# A8054
Picrotoxin (PTX)	Sigma-Aldrich	Cat# P1675
Tetrodotoxin (TTX)	Enzo Life Sciences	Cat# BML-NA120-0001
Artemisinin	Sigma Aldrich	Cat# 361593
Artemether	Sigma Aldrich	Cat# A9361
Artesunate	Sigma Aldrich	Cat# A3731
Nocodazole	Santa Cruz Biotechnology	Cat# sc-3518
(1,2,5,6-Tetrahydropyridine-4-yl) methylphosphinic acid	Tocris	Cat# 1040
Glucose Oxidase from <i>Aspergillus niger</i>	Sigma Aldrich	Cat# G2133
Cysteamine	Sigma Aldrich	Cat#30070
Catalase from Bovine liver	Sigma Aldrich	Cat#C40
DNase 1	Sigma-Aldrich	Cat# D5025
B-27 supplement	GIBCO	Cat# 17504-010
Cytosine Arabinoside (Ara-C)	Sigma	Cat# C6645
Transferrin	Calbiochem	Cat# 616420
Experimental models: Organisms/strains		
Sprague-Dawley rat pups (P1-P2)	Charles River	Strain code: 400
Software and algorithms		
MiniAnalysis	Synaptosoft	http://www.synaptosoft.com/MiniAnalysis
Clampfit	Molecular Devices	http://www.moleculardevices.com
Prism	GraphPad	http://www.graphpad.com

REAGENT or RESOURCE	SOURCE	IDENTIFIER
Antibodies		
Vutara VXL software	Bruker	N/A
MATLAB	Mathworks	https://www.mathworks.com/products/matlab.html
Intellicount	Fantuzzo et al., 2017	N/A
Fiji	ImageJ processing package – open source	https://imagej.net/Fiji

Author Manuscript

Author Manuscript

Author Manuscript

Author Manuscript